Bull Earthquake Eng (2014) 12:939–960
DOI 10.1007/s10518-013-9552-2

ORIGINAL RESEARCH PAPER

Performance-based seismic design of integral abutment bridges

Paolo Franchin · Paolo Emilio Pinto

Received: 16 November 2012 / Accepted: 3 November 2013 / Published online: 21 November 2013

Abstract Integral abutment bridges (IAB) are experiencing increasing diffusion in the short to mid-range lengths, where they offer some advantages over traditional girder bridges with non-monolithic connection at the abutments. One challenging problem with their analysis and design is that consideration of the interaction between foundation soil, structure and backfill is unavoidable, also for the deck design. Further, the end of the construction is only one of the conditions that need to be verified during design. Cyclic deformations, such as those occurring during ground shaking, typically lead to an increase in stresses in the abutments and connections, due to progressive compaction (ratcheting) of the backfill soil. This problem is magnified when the bridge is comprised between two embankments, whose response may amplify the input motion and drive the deformation of the bridge. Performance-based design aims at superseding current design procedures by explicitly checking that the target performances set out are achieved, and not overly exceeded. Such a design paradigm naturally calls, on the one hand, for improved accuracy in response determination and more refined analyses, and, on the other, for taking into account the uncertainties entering into the problem by means of an explicitly probabilistic approach. With this objective in mind, the paper presents an inelastic dynamic model for the seismic analysis and design of IABs. The model, that features a balanced compromise between the setup and evaluation effort on one hand, and accuracy on the other, has been developed for implementation in typical commercial analysis packages. It builds on 1D site-response analysis and on inelastic Winkler-like modeling, to reproduce the main physical aspects of the seismic response of IABs. One example application to a highway overpass in Italy illustrates the model and the relevance of a fully probabilistic approach to performance-based design. The application offers also important insight into the choice of an efficient intensity measure for this type of structure.

P. Franchin (✉) · P. E. Pinto
Department of Structural and Geotechnical Engineering, University of Rome "La Sapienza",
Via Antonio Gramsci 53, 00197 Rome, Italy
e-mail: paolo.franchin@uniroma1.it

P. E. Pinto
e-mail: pinto@uniroma1.it

Keywords Uncertainty · Probability · Ratcheting · Inelastic cumulative displacements · Embankment · Amplification · Optimal intensity measure

1 Introduction

The paper focuses on seismic design of a particular structural typology that has gained increased interest worldwide, i.e. the integral abutment bridge (IAB). As it is well known, the advantage of this typology consists in the elimination of joints and bearing devices at the abutments by realizing a monolithic connection between deck and abutment wall. This translates into both lower construction and maintenance costs.

The country with the largest number of IABs is by far the USA, where the typology has been in widespread use for more than twenty years (Burke 1990), and it is reported that more than 13,000 such bridges (Maruri and Petro 2005) where built already in 2005. A relatively recent overview of US practice is provided by (Wasserman 2007), who dates the first realizations in some states (Ohio, South Dakota and Oregon) to as far back as in the 1930s and ‘40s. Moving to Europe, it is recognized that this typology has been employed in Switzerland for more than half a century now, since it was the mainstream choice for the bridges on the highway network built after WWII (Kaufmann 2011). An overview of the different European practices is given in White et al. (2010). White (2007) also previously compared European with US practice. IABs have been considered and realized in many other countries, e.g. in Japan (Nakamura et al. 2002; Akiyama and Kajikawa 2008), and in Australia (Connal 2004).

In view of the large number of realizations worldwide, one would expect that a consolidated design practice and guidelines would be available. On the contrary, indications are missing even in modern codes, in particular for the specific aspect of seismic design. This can be attributed to a good extent to the fact that, from an analysis and design point of view, the structural continuity existing between deck, abutment wall and supporting piles makes essential full consideration of soil–structure interaction (SSI) phenomena, an area which still requires specialized expertise and is not satisfactorily amenable of simplified procedures to be used in practice.

Consideration of SSI is essential for both seismic action and service loads. With respect the latter, one aspect peculiar to this typology is the fact that independently of the presence of loads, the cyclic thermal excursions of the deck (England et al. 2000) occurring during the entire service life lead to a progressive build-up of earth pressures behind the abutments, which may reach very large levels at the occurrence of seismic actions. Furthermore, the relevance of SSI becomes dominant in case of elevated bridges, e.g., overpasses, due to the presence of the embankments at their ends. These latter are in fact additional components of the whole system, having a seismic response of their own that in many cases drives the response of the bridge itself. Notably, the fact that embankment contribution is entirely neglected even in modern codes, such as Caltrans (1999) and ATC (1996a,b), confirms the lack of established methods (Kotsoglou and Pantazopoulou 2007).

Nonetheless, papers on the analysis of these bridges are relatively abundant in the technical literature. A review of the methods, however, reveals the actual scarcity of comprehensive approaches, contrasting with the larger number of papers dealing with specific, partial aspects of the whole problem.

Spyrakos and Loannidis (2003) concentrate on the longitudinal response of a prestressed concrete IAB, carrying out modal analysis on an equivalent linear model (iterative) excited only at the base, with the aim of assessing the contribution of SSI to the response. Dicleli

(2005) also considers the longitudinal response of IABs and focuses on the effect of cyclic thermal movements. He employs pushover analysis on a model with nonlinear soil springs and piles and, based on parametric analyses, derives design equations for the maximum allowable length as a function of abutment strength. The maximum deck length is a debated issue, see e.g. (Baptiste et al. 2011). In practice, very different lengths are encountered in past realizations: Wasserman (2007) reports limitations in the US varying from state to state, but indications tend to agree on a limit between 400 and 500 m. Pekcan et al. (2010) focus on the design of the deck-abutment connection in steel IABs, employing refined nonlinear FE models of the connection to derive the flexibility of the connection spring used in a global 3D frame model of the bridge. They also consider the bridge excited at its base neglecting embankment amplification. Similarly, Vashegani-Farahani et al. (2010) assess the longitudinal response of a composite steel-concrete deck IAB by means of inelastic time-history analysis of a 3D frame model. They employ nonlinear interaction springs that connect the structure with a fixed support (again, no embankment amplification), and evaluate the influence of the backfill compaction level. A step towards consideration of the motion amplification is that presented in Dicleli and Erhan (2011), where a fairly comprehensive 3D model of an IAB is employed in inelastic time-history analysis. Notably, however, the abutment wall is connected with an assembly of springs to a rigid support. Kotsoglou and Pantazopoulou (2007, 2009, 2010) highlight the importance of the embankment dynamic properties in the response of IABs, focusing on the transverse response. They employ refined 3D finite element models and compare them with shear wedges to derive the dynamic impedance properties of embankments, which they then use in a IAB model according to a sub-structuring approach. Zhang and Makris (2002a,b) similarly consider the dynamic response of embankments and employ shear wedge and complete 3D finite element models for the purpose.

The above brief overview shows that there is still room for improvement in modelling of these structures, especially with the aim of devising models that capture the fundamental physical aspects and response characteristics of IABs, without resorting to tools that cannot be used in practice for design, and can be regarded as high-ended even at the research level (Elgamal et al. 2008). Further, even though in some cases parametric studies have been conducted on the effect of some system parameters, proper consideration of the uncertainty affecting both system properties and the seismic excitation is not present in the cited works. This, on the other hand, is an essential aspect of a thorough implementation of the performance-based design (PBD) paradigm.

It is observed, however, that even current formulations for design against seismic action, e.g. (CEN 2004; CEN 2005 IBC 2012), though they are well conceived and tested and claim to be PBD procedures, fall short of providing a measure of actual compliance with the stated performance objectives. In view of the several unavoidable sources of uncertainty affecting the problem, such a measure should be properly given in probabilistic terms.

The last decade has seen reliability methods for seismic design become effective tools that can be used in practice with an acceptable amount of additional effort and competence (Cornell 1996; Cornell and Krawinkler 2000; Krawinkler and Miranda 2004).

Based on the previous discussion, this paper presents a fully probabilistic PBD approach for seismic design of IABs. The approach results in the mean annual frequency (MAF) of exceedance λ of any response quantity of interest (stress resultants for strength design, cumulative displacements and deformations), from which an appropriate design value, characterized by an accepted MAF of exceedance, can be chosen. The approach employs inelastic response history analysis (IRHA) for a number of recorded ground motions. Its practical applicability rests on the use of a simplified treatment of the nonlinear dynamic behavior of the soil–structure system, previously developed by the authors for the analysis of diaphragm

walls (Franchin et al. 2007), and adapted to the IAB case. With respect to the previously cited works, the method accounts for uncertainty in both system properties and seismic action (intensity, frequency content, duration), and the model can describe the input motion amplification through both the foundation soil and the embankment, as well as the inelastic interaction between soil-backfill and structure, resulting in progressive accumulation of pressures, displacements and internal forces. Section 2 describes the model, Sect. 3 introduces the probabilistic PBD procedure, while Sect. 4 illustrates their application to a highway overpass in Italy.

2 Model

Figure 1 shows a single-span integral-abutment highway overpass (left) and its numerical model (right). Three main elements can be identified in the system: (a) the structure, composed of the deck and the abutments, (b) the soil close to the structure, whose response is influenced by the interaction with the structure, (c) soil outside this region, whose motion can be considered undisturbed by the structure (free-field). In particular, element (b) consists of the portions of the natural foundation soil in which the piles are embedded, and of the embankment on top of it, in direct contact with the abutment wall.

In seismic conditions the structure is deformed by the motion of the foundation soil and of the embankment on top of it. As it has been already noted, the vibration of the embankment may well drive the motion of a short bridge and completely dominate its response.

In the assumption that the seismic motion consists of vertically propagating shear waves, the proposed model is based on the non-linear shear-beam approximation for the response of the ground layers and of the embankments on both sides of the bridge. In particular, the shear-beam on each side of the bridge is comprised of two parts: the lower one, corresponding to the natural foundation soil, has a constant cross-section, while the upper one, corresponding to the embankment, is tapered towards to the crest.

The shear-beam motion is input to the structure (piles and abutment wall) through springs for which the well-known one-dimensional nonlinear Winkler approximation is adopted. The latter approximation has been subjected to a limited validation versus the results of inelastic 2D finite element analysis with reference to diaphragm walls (Franchin et al. 2007). The results therein show how the model is capable of providing reasonably good predictions for both maximum and residual bending moments, as well as for cumulative displacements.

The elements of the model are schematically depicted in Fig. 2, which shows also the required input parameters. The denomination of the employed finite elements typologies follows that of the commercial analysis package SAP2000, version 14.1 (CSI 2009), used to

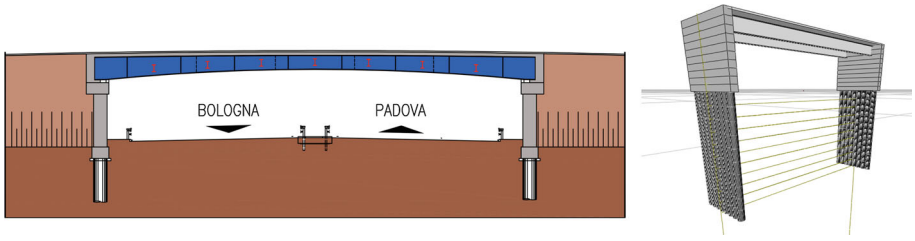

Fig. 1 Typological highway overpass on the Italian A13 highway (*left*) and corresponding analysis model (*right*, only structural portion shown)

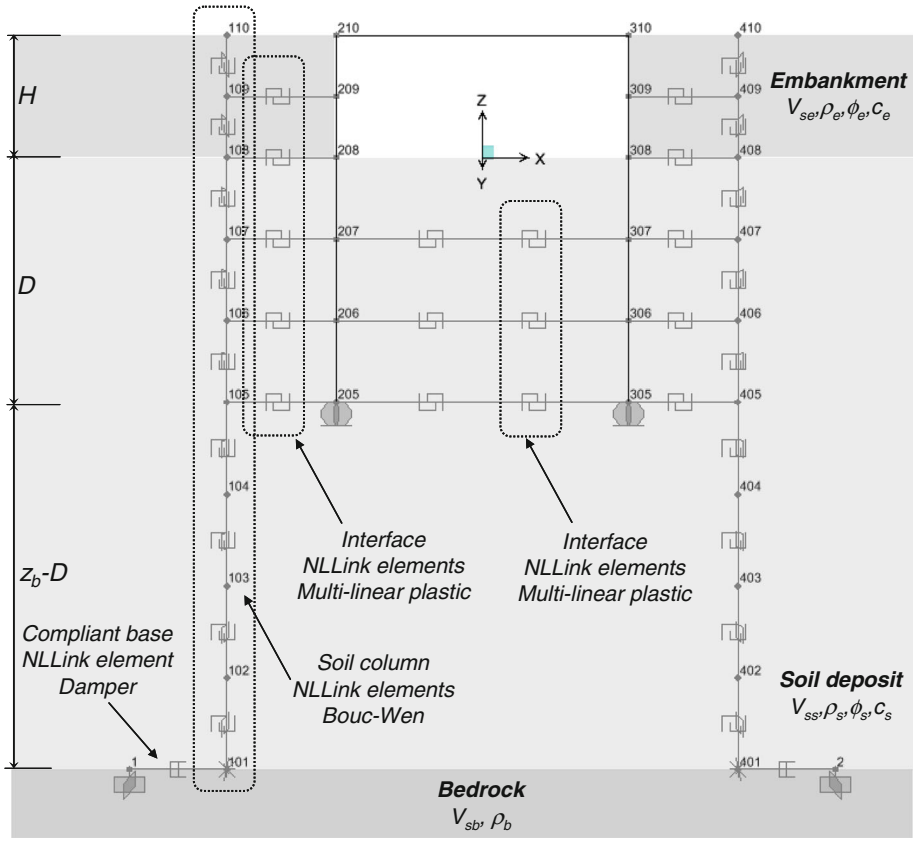

Fig. 2 Model components and parameters

implement the model for the application in Sect. 4. The seismic motion is input at the base, as explained in Sect. 2.5 and shown in Fig. 4.

2.1 Foundation soil

Two twin 1D soil columns on both sides of the bridge extend from the bedrock to the deck level. These columns are those that are commonly used in site response analysis. The state of practice of one-dimensional site response analysis is mostly based on the equivalent linearization approach in the frequency domain introduced in Schnabel et al. (1972), implemented in codes such as SHAKE or EERA. The limit of this approach in relation to the analyzed system and to performance-based design, however, is that it cannot predict residual displacements. This is the reason for adopting time-domain inelastic analysis. Hysteretic constitutive laws for soils are commonly specified in terms of a monotonic backbone, either hyperbolic or derived from modulus degradation curves, to which a predefined unload-reload rule is attached, e.g. the Masing criterion (Kramer 1996). This basic inelastic model, however, is known to be capable of reproducing experimentally derived secant stiffness but also to overestimate the equivalent damping at higher strain levels. More refined models that reproduce both stiffness and damping correctly are available and implemented in codes such as Cyclic-1D (Elgamal

et al. 1998), primarily employed for liquefaction-susceptible soil profiles, and NL-DYAS (Gerolymos and Gazetas 2005; Drosos et al. 2012). The former employs a multi-surface plasticity model, while the latter employs an enhanced variant of the well-known Bouc-Wen (BW) model (Bouc 1971; Wen 1976), denominated BWGG. Both can model cyclic degradation and even cyclic mobility in saturated coarse-grained soils. They yield basically equivalent results, as shown in Drosos et al. (2012).

The approach followed herein is the same as in Franchin et al. (2007) and employs a simplified variant of the Bouc-Wen model, which is that implemented in the adopted commercial code Sap2000. In particular, the soil columns are modeled with *NLLink* elements (here used as 1D shear springs) to which the *Wen* plasticity law is assigned to describe the shear force-deformation response. The *Wen* law implemented in Sap2000 is the simple symmetric one without pinching, and stiffness or strength degradation, governed by the equations:

$$f = \alpha k u + (1 - \alpha) f_y z \tag{1}$$

$$\dot{z} = \begin{cases} \dot{u} \left(1 - \lfloor z \rfloor^n\right) & \text{if } z\dot{u} > 0 \\ \dot{u} & \text{otherwise} \end{cases} \tag{2}$$

where f is the force, u the displacement and z is an internal variable whose evolution is governed by the differential equation (2) and determines the shape of the hysteresis loop. The model has four parameters: the initial stiffness k, the hardening ratio α, the yield displacement u_y and the exponent n which regulates the sharpness of the transition between the elastic and the post-elastic behavior. Equation (2) is obtained from the complete equation of the basic BW model:

$$u_y \dot{z} = \dot{u} \left[1 - |z|^n \left(\beta + \gamma \operatorname{sgn}\left(z\dot{u}\right)\right)\right] \tag{3}$$

by setting $\beta = \gamma = 0.5$ which corresponds to a Masing criterion for the unload-reload curve (Drosos et al. 2012). The corresponding approximation, which is due to the present capabilities of the employed analysis code, is recognized.

Soil deposits exhibit different variations of strength and stiffness (which are closely related) with the effective confinement pressure $\sigma_0' = \sigma_0'(z)$, depending on their plasticity index PI. In particular, coarse-grained soil with low PIs have both stiffness and strength generally increasing with depth, while fine-grained soils with high PIs tend to have constant stiffness and strength (Ishibashi and Zhang 1993). Accordingly, the model allows depth-dependent values to be assigned to k and f_y according to the following expressions:

$$k(z) = \frac{G_0(z) A}{\Delta z} \tag{4}$$

$$f_y(z) = A \tau_y(z) \tag{5}$$

where G_0 is the initial shear modulus of the soil or embankment material, A is the column cross-section area, Δz is the layer thickness and τ_y the shear strength of the soil material. The initial shear modulus can be derived either from correlations with SPT and CPT data, or using the relation $G_0(z) = \rho(z) V_s^2(z)$ with the mass density ρ and the shear wave velocity V_s. The shear strength can be obtained again from correlation with in-situ tests or, for example, as $\tau_y(z) = G_0(z) \gamma_y(z)$ where $\gamma_y(z)$ is the depth-dependent yield shear strain of the soil material. The latter parameter is tabulated as a function of σ_0' and PI in Drosos et al. (2012). Herein the simple Mohr-Coulomb model has been used and hence:

$$\tau_y(z) = c(z) + \sigma_0'(z) \tan\phi(z) \tag{6}$$

where c and ϕ are the cohesion and internal friction angle of the soil material.

The other parameters of the Wen model have been set constant and equal to $n = 2$ (corresponding to a smooth, rounded transition between elastic and plastic branches) and $\alpha = 0$ (no hardening). These are both within the typical ranges of these parameters indicated in Drosos et al. (2012): n between 0 and 5, β between 0.4 and 0.6 and α between 0 and 2 %. Finally, each layer has mass $m = \rho$ A Δz.

2.2 Embankments

It is noted that for the portion of the column describing the foundation soil (z < 0), the area A is constant and chosen to be "large enough", so that its motion is not influenced by the interaction with the enclosed bridge or the embankment response. The portion of the column above ground (0 < z < H), corresponding to the embankment (see Fig. 2), has a trapezoidal transverse shape and hence the 1D beam elements have decreasing cross-section area toward the top, according to the shear wedge model introduced by Wilson and Tan (1990a,b). The dimension of the embankment elements parallel to the X axis (longitudinal axis of the bridge, see Fig. 2) has been set equal to:

$$L_c \cong 0.7\sqrt{SB_cH} \tag{7}$$

where B_c and B_b are the crest and base width of the embankment, and $S = 2H/(B_b - B_c)$ is its slope. The above expression is the result of a study on the use of lower-order models for the determination of the dynamic response of earth embankments (Zhang and Makris 2002a,b). The study has compared dynamic properties of a 3D model of a long embankment (both prismatic and sloping along the longitudinal axis X) with that of a 1D tapered shear beam and found that the above length yields frequency transfer functions, in both the longitudinal and transverse directions, that exhibit a quite good match with those obtained with the full model.

2.3 Interface and structural elements

The portion of soil in direct contact with the structure is denominated "interface" and consists of four sets of springs modeling, from left to right (see Fig. 2): (a) the contact between the left column and the left abutment/piles, (b) the contact between the piles of the left abutment and the soil enclosed within the abutments, (c) and (d) the analogous contacts on the right side. It should be noted that the springs (b) and (c) are connected directly to the opposite column (e.g. a spring goes from joint 205 to 405, and a spring goes from joint 305 to 105). This, coupled with a kinematic constraint that forces the two columns to have the same displacement at each level z, amounts to saying that these springs work on the relative displacement of the piles with respect to the free-field motion, and neglecting in approximation the difference in motion between the free-field and the soil enclosed by the two pile diaphragms.

NLLink elements are used also for these interaction springs. These elements can be assigned independent 1D constitutive laws on the six degrees of freedom. A *MultiLinearPlastic* axial force-deformation law is assigned to the horizontal degree of freedom, while a *Linear* shear force-deformation law is assigned to the vertical degree of freedom. The latter is employed to model the distributed vertical load-transfer between piles and surrounding soil, and the corresponding stiffness is equal to:

$$k_Z(z) = n_p 0.6E(z)\left[1 + 0.5\sqrt{a_0}\right] \tag{8}$$

where n_p is the number of piles, $E(z) = 2(1 + \nu)G_0(z)$ is the Young modulus of soil (ν is its Poisson ratio, set equal to 0.3 in the application) and $a_0 = \omega d / V_s(z)$ is the non-

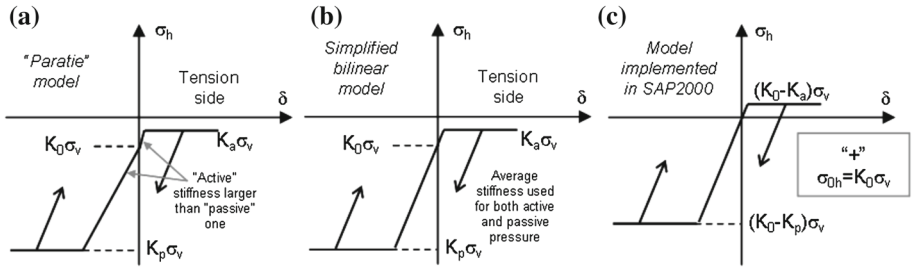

Fig. 3 Constitutive law for the interface elements

Fig. 4 Loading stages

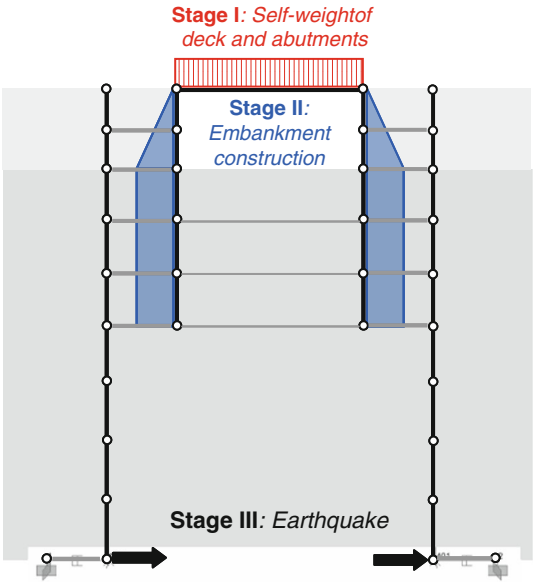

dimensional frequency parameter. The frequency-dependence of the stiffness is mild in the range of frequencies of interest: a constant value is used for the purpose of time-domain analysis, setting $\omega = 2\pi / T_1$, where T_1 is the fundamental period of the deposit.

As far as the horizontal degree of freedom is concerned Fig. 3 shows three inelastic constitutive laws: (a) schematically represents the constitutive law presented in Becci and Nova (1987) at the basis of the analysis package "Paratie", widely employed in Italy for the Winkler-type analysis and design of flexible diaphragm walls; (b) is the approximation adopted in Franchin et al. (2007) for the purpose of inelastic dynamic analysis of diaphragm walls within the analysis package OpenSEES (McKenna et al. 2000), where a single stiffness value is adopted for both active and passive earth pressure conditions; (c) is the approximation adopted herein due to SAP2000 requiring *NLLink* elements to have a force-deformation law that passes through the axes origin ($f = u = 0$). In order to comply with this requirement the "K_0" (at-rest) stresses are recreated with a pattern of horizontal forces applied in the walls nodes, labeled 200's and 300's in Fig. 2 (see also the following Fig. 4).

Depth-dependent values are assigned to stiffness and strength according to the following expressions:

$$k_x(z) = 1.2\frac{E(z)\,A_c(z)}{L} \tag{9}$$

$$f_y^+(z) = -A_c(z)\,[K_a(z) - K_0(z)]\,\sigma_v(z) \tag{10}$$

$$f_y^-(z) = -A_c(z)\left[K_p(z) - K_0(z)\right]\sigma_v(z) \tag{11}$$

where $A_c(z) = B_d \Delta z(z)$ is the contact area, where B_d is the deck width assumed to be equal to the abutment width; $L = (L_a + L_p)/2$ is the average of the passive and active lengths, as defined in "Paratie" for the purpose of stiffness determination (i.e. the stiffness is assigned a common average value for active and passive pressure conditions):

$$L_a = \frac{2}{3} l_a \tan\left(45° - \frac{\phi}{2}\right) \text{ with } l_a = \min(\mathrm{H} + \mathrm{D}, 2\mathrm{H}) \tag{12}$$

$$L_p = \frac{2}{3} l_p \tan\left(45° + \frac{\phi}{2}\right) \text{ with } l_p = \min(\mathrm{D}, \mathrm{H}) \tag{13}$$

For the earth-pressure coefficients in at rest, active and passive conditions, the following basic expressions have been used in the application:

$$K_0 = 1 - \sin\phi \tag{14}$$

$$K_a = \frac{1 - \sin\phi}{1 + \sin\phi} \tag{15}$$

$$K_p = \frac{1 + \sin\phi}{1 - \sin\phi} \tag{16}$$

While the foundation soil is a natural medium that will respond to seismic input of increasing intensity eventually entering in the nonlinear range, the structure is the object of a design with prescribed performance objectives. Most current seismic design codes prescribe elastic response for the foundation structures and in general for structures in contact with soil, such as diaphragm walls. Furthermore, the recent trend in bridge design is to make reduced if any resort to inelastic reserves, in recognition of the strategic character of these structures in the resilience of communities, and considering also the limited extra cost associated with this choice. Structural members are modeled with *frame* elements. These can be either linear or nonlinear, depending on the target performance under seismic action. If elastic response is desired, frame elements are linear and the response in terms of stress resultants is used to design strength. Conversely, if exploitation of ductility is accepted, strength is designed for gravity and traffic loads, and nonlinear frame elements can be used for a displacement-based verification under seismic action. Nonlinear frame elements are also necessary when assessing an existing structure.

2.4 Input motion

As far as the seismic motion is concerned, this is input to the system through a compliant base in terms of forces (see next section, and Fig. 4) proportional to ground velocity:

$$f(t) = c_b \dot{u}(t, z_b) \tag{17}$$

in which the base damper constant is assigned the value $c_b = \rho_b V_{sb} A$, where the mass density and shear wave velocity are those of the elastic bedrock and A is the soil column cross section area (Kramer 1996). The velocity at depth z_b is obtained integrating the acceleration history,

which in turn is the deconvolution of the surface signal. The latter operation is repeated for all ground motions in the suite selected for the purpose of the probabilistic analysis described in the following Sect. 3.

Selection of natural motions for the purpose of inelastic dynamic analysis is a topic of ongoing discussion since the late '90s (Shome et al. 1998). As explained in Sect. 3 (Eqs. 18, 19), MAF of exceedance of response thresholds of interest are computed according to the total probability theorem, employing as an intermediate (conditioning) variable a measure of intensity of the seismic motion, commonly denoted as IM. It is well known that if the latter is "sufficient", i.e. it makes the response unconditional on all other ground motion properties, the choice of records can be done in a relatively free manner (Shome et al. 1998). Since, however, there cannot be a perfectly sufficient IM for general nonlinear multi-degree of freedom system, it is an accepted fact that the selection of records should be such as to reflect the seismicity of the site. This can be done in different ways, of varying complexity. The "softer" approach would be that of targeting the causative magnitude and distance ranges of the events that dominate the hazard at the site, as provided by probabilistic seismic hazard analysis (PSHA) de-aggregation. These ranges depend on the chosen IM and hazard level and it is often suggested to use levels close to the final value of the MAF. PSHA de-aggregation actually yields triplets of values, including also the so-called "epsilon", beside magnitude and distance. Epsilon measures the distance of a motion from the average one for the considered magnitude and distance. There are proposals to consider epsilon in the record selection, because it is a good predictor of the spectral shape (Baker and Cornell 2006).

The above selection criteria in most cases translate in a correct representation of duration properties, not included in spectral IMs (the mainstream choice), which are very relevant to degrading hysteretic systems, such as e.g. existing structures or systems that are sensitive to cumulative energy, like the IAB.

Finally, in order to carry out the deconvolution to the model base with the same profile for all motions, the latter need to be selected, with the previous criteria, within a pool of records from rock/stiff soil conditions.

2.5 Load stages

The nonlinear analysis requires a sequence of three load stages, as shown in Fig. 4. The seismic input is applied last to the system (Stage III), after the gravity loads of the deck (Stage I) and the increment of earth pressures (Stage II) due to the construction of the embankment. The latter is linearly increasing from z = H to z = 0, and constant there on. For simplicity, the model does not change from one stage to the next one (i.e. it is not a sequential construction analysis): the interface springs properties (sets *a* and *d*) during Stage I should account for the absence of the embankment.

3 Probabilistic seismic performance-based design

As stated in the introduction, the final result of the method is the MAF of exceedance of any force or deformation design quantity of interest. With reference for instance to an elastic target performance and to the bending moment at the abutment-deck connection, the design value is the maximum attained during Stage III, M_{III}, which can be expressed as the sum of the moment at the end of Stage II, M_{II}, and of the moment increment Δ M, both of which are in general random quantities. Accordingly, the MAF of $M_{III} = M_{II} + \Delta M$ can be expressed by the theorem of total probability as:

$$\lambda_{M_{III}}(x) = \int_{S_a=0}^{\infty} \int_{M_{II}=0}^{\infty} G_{\Delta M|S_a,M_{II}}(x - z|\, y, z) \underbrace{f_{M_{II}}(z)\, dz}_{p(M_{II}=z)} \left| d\lambda_{S_a}(y) \right| \tag{18}$$

which expresses the fact that, for any intensity level $S_a = y$, M_{III} exceeds x whenever M_{II} equals z and ΔM exceeds $x - z$. The functions G, f and λ_{Sa} are the complementary cumulative distribution function (CCDF) of the seismic moment increment, conditional on the seismic intensity and Stage II moment, the probability density of M_{II}, and the MAF of exceedance of the seismic intensity (seismic hazard curve), respectively.

In the simple case that the variability of M_{II} is negligible with respect to that of ΔM, the previous equation simplifies to:

$$\lambda_{M_{III}}(x) = \int_{S_a=0}^{\infty} G_{\Delta M|S_a}(x - M_{II}|\, y) \left| d\lambda_{S_a}(y) \right| \tag{19}$$

The seismic intensity in the above equations is expressed in terms of a single scalar intensity measure, which is here chosen to be a spectral acceleration. Its probability distribution is given by the seismic hazard curve λ_{Sa}, which is the end result of a probabilistic seismic hazard analysis. The period at which Sa is evaluated is often taken equal to the fundamental period of the system, $S_a = S_a(T_1)$, which in the case at hand would nearly coincide with that of the soil deposit (given the ratio of masses between the soil column and the bridge). This is not found to be the optimal choice for IABs and a discussion and indications are given in Sect. 4 with reference to the application results.

The CCDF of the seismic moment increment can be expressed, under the assumption that ΔM is lognormal, as:

$$G_{\Delta M|S_a}(x - M_{II}|\, y) = 1 - \Phi\left(\frac{\ln(x - M_{II}) - \mu_{\ln \Delta M|S_a=y}}{\sigma_{\ln \Delta M|S_a=y}} \right) \tag{20}$$

where $\mu_{ln}\Delta_{M|y}$ and $\beta = \sigma_{ln}\Delta_{M|y}$ are the mean and standard deviation of the logarithm of ΔM. It is common to model the median of ΔM as a power-law function of the intensity, with parameters a and b:

$$(\Delta M|\, S_a)_{50\%} = a y^b \rightarrow \mu_{\ln \Delta M|S_a=y} = \ln a + b \ln y \tag{21}$$

and to consider the "dispersion" $\beta = \sigma_{ln\Delta_{M|Sa=y}}$ independent of S_a. The complete probabilistic characterization of the seismic demand reduces then to the evaluation of the three parameters: a, b and β. This can be done in an affordable manner employing linear regression on the results of n (a few tens) of inelastic response history analyses (IRHA) with unscaled recorded motions. As shown in the application, the analysis can also easily incorporate the uncertainty in system properties, such as soil/embankment stiffness and/or strength.

When the variability of M_{II} is not negligible, the full CCDF of ΔM conditional on S_a and M_{II} is needed. This can be obtained as follows under the assumption that $\Delta M(y)$ and M_{II} are jointly lognormal. In this case the marginal distribution of ΔM remains the same as in Eq. (21), while M_{II} is lognormal with parameters μ_{lnMII} and σ_{lnMII}. The parameters of the conditional distribution can be found as (Benjamin and Cornell 1970):

$$\mu_{\ln \Delta M|S_a=y,M_{II}=z} = \mu_{\ln \Delta M|S_a=y} + \rho_{\ln \Delta M|S_a=y,\ln M_{II}} \frac{\sigma_{\ln \Delta M|S_a=y}}{\sigma_{\ln M_{II}}} \left(\ln z - \mu_{\ln M_{II}} \right) \tag{22}$$

$$\sigma_{\ln \Delta M|S_a=y,M_{II}=z} = \sigma_{\ln \Delta M|S_a=y} \sqrt{1 - \rho_{\ln \Delta M|S_a=y,\ln M_{II}}} \tag{23}$$

where, consistently with the use of a constant value for the dispersion $\beta = \sigma_{\ln \Delta M|S_a=y}$, a constant value independent of S_a is also employed for $\rho_{\ln \Delta M|S_a=y,\ln M_{II}}$, evaluated on the basis of a finite number n of analyses as:

$$\rho_{\ln \Delta M|S_a=y,\ln M_{II}}, = \frac{\frac{1}{n-p}\sum_{i=1}^{n}\left(\ln M_{II,j} - \mu_{\ln M_{II}}\right)\left(\ln \Delta M_i - (\ln a - b \ln y_i)\right)}{\beta \sigma_{\ln M_{II}}} \tag{24}$$

The design value for the total moment M_{III} (action effect) is obtained inverting Eq. (18) or (19) for an assigned accepted value λ_0 of its MAF of exceedance: $M_{III,d} = x(\lambda_0)$. The corresponding mean strength (ultimate moment evaluated with mean material properties) is finally designed amplifying $M_{III,d}$ by the factor $\exp(-0.5\beta_C^2 k/b)$ that accounts for the uncertainty in the strength β_C, and for the hazard and demand exponents k and b (see for details Cornell et al. 2002).

4 Application

The procedure illustrated in the previous section has been applied to the highway overpass in Fig. 1. The overpass is a tentative standard design solution to be used for the upgrade works on Italian highways A13 "Bologna-Padova" and A12 "Roma-Civitavecchia". This overpass has been located for the purpose of this example at the beginning of A13 close to Bologna (44.53°N − 11.36°E). According to the Italian design code, this structure should be designed to remain elastic under a seismic action characterized by a mean return period of about 1,000 years. Accordingly, in this application in order to evaluate the elastic demand for strength design the structure (frame elements of the deck and abutment wall and piles) is modeled as linear elastic. Recourse to inelastic dynamic analysis (inelasticity is considered in the soil and embankment) of this typological design, and of similar ones, is due to concerns about their seismic behavior, in particular about possible detrimental effects of embankment-driven deformations.

The deck has composite steel-concrete section (two steel girders and a 12.00 m wide concrete slab, for a span length of $L = 38.00$ m), and the abutments are solid RC walls (1.20 m thick, of height $H = 10.00$ m) founded over a RC pile diaphragm ($8\,\phi\,1,200$ piles at 1.35 m, of length $D = 20.00$ m).

The *foundation soil* is assumed to be a homogeneous dense sand with a constant unit weight $\gamma = 20\,\text{kN/m}^3$, shear wave velocity increasing with depth according to $V_{ss} = cz^{\text{m}} = 170z^{0.25}$m/s (which corresponds to an average shear wave velocity over the first 30 m equal to $V_{ss} \approx 320$ m/s), friction angle $\phi = 30°$ and negligible cohesion. The soil layer extends for 50 m down to an elastic bedrock with unit weight $\gamma = 20\,\text{kN/m}^3$ and average shear wave velocity $V_{sb} = 1,000$ m/s, leading to a damper constant $c_b = 5.14 \times 10^7$ kNs/m. The embankment soil is a slightly lighter and softer material, with unit weight $\gamma = 18\,\text{kN/m}^3$, average shear wave velocity $V_{se} = 250$ m/s, friction angle $\phi_e = 30°$ and a cohesion $c = 1$ kPa.

Since uncertainty on a new structure designed for elastic response is much lower than that associated to inelastic response of natural soil, uncertainty in the former is not modelled. Two cases are considered. The first, labeled "Mean model", in which no uncertainty on the soil properties is considered, and the model is set up with the values above. The second case, labeled "Random soil", is included to show how the effect of uncertainty in soil stiffness and strength can be considered. In this latter case, for illustration purposes, four properties are modeled as random variables as two statistically independent vectors: the first one includes the coefficient c in the V_{ss} power law, taken uniform in the interval [110,220], and the friction

Table 1 Selected ground motions

Record	Event	Event name	Year	Station	M	R_{epic}(km)	D(s)	D_{eff}(s)
1	1	Chi-Chi, Taiwan-02	1999	TCU067-N.at2	5.9	33.9	61	25
2	1	Chi-Chi, Taiwan-02	1999	TCU071-N.at2	5.9	23.1	52	25
3	1	Chi-Chi, Taiwan-02	1999	TCU075-N.at2	5.9	34.1	54	25
4	1	Chi-Chi, Taiwan-02	1999	TCU076-N.at2	5.9	34.2	45	20
5	2	Coalinga-01	1983	H-Z06000.at2	6.4	42.8	40	25
6	2	Coalinga-01	1983	H-Z09000.at2	6.4	41.2	32	30
7	2	Coalinga-01	1983	H-Z10000.at2	6.4	41.4	40	30
8	3	Griva, Greece	1990	L-EDE-NS.at2	6.1	32.9	28	15
9	4	Irpinia, Italy	1980	B-AUL000.at2	6.2	37.2	32	32
10	4	Irpinia, Italy	1980	B-BAG000.at2	6.2	22.3	42	30
11	5	Morgan Hill	1984	CLS220.at2	6.2	30.1	36	20
12	5	Morgan Hill	1984	SJL270.at2	6.2	57.7	28	28
13	6	N. Palm Springs	1986	SIL000.at2	6.1	27.7	24	15
14	7	Parkfield	1966	C12050.at2	6.2	36.2	44	44
15	7	Parkfield	1966	TMB205.at2	6.2	40.3	30	12
16	8	Santa Barbara	1978	CAD250.at2	5.9	34.0	11	7
17	9	Sierra Madre	1991	chan1155.at2	5.6	18.7	40	8
18	10	Whittier Narrows	1987	A-CHL030.at2	6.0	37.1	16	10
19	10	Whittier Narrows	1987	A-MU2032.at2	6.0	31.1	32	16
20	10	Whittier Narrows	1987	A-TUJ262.at2	6.0	29.5	31	16

angle $\phi_s \sim U(27, 33)$, with an assumed correlation coefficient of 0.8; the second vector includes the constant shear wave velocity of the embankment material $V_{se} \sim U(200, 300)$ and the corresponding friction angle $\phi_e \sim U(28, 32)$, with an assumed correlation coefficient of 0.8. It is noted how this simplified characterization of the variability of the soil profile is used here just as an example, while the method itself allows without effort to treat more realistic and complex models (Franchin and Cavalieri 2013). One random sample of the four variables is associated to each of the recorded ground motion used for the analysis.

Variability in the input motion is described through a suite of 20 recorded ground motions. Table 1 reports the records, selected from the PEER strong motion catalogue in a magnitude bin between 5.5 and 6.5. The latter corresponds roughly to the magnitude range expected at the site from the employed PSHA de-aggregation. The latter should be the de-aggregation of the chosen IM for a return period close to the inverse of the final MAF. Since the complete de-aggregation data were not available for the considered site, the (M, R) bin for the 500-year PGA de-aggregation (provided for the entire national territory in Italy by the National Institute for Geophysics and Volcanology) was used in approximation. Records were selected from rock outcrop and stiff-soil ($V_S > 800$ m/s). Table 1 reports also duration and effective duration, used to terminate the analysis.

Figure 5 shows an example of the results that are obtained from the model, with reference to the "Mean model" and record #17 (the record inducing the largest seismic moment increment in the right deck-abutment connection). The figure shows the bending moment envelope over the three analysis stages, and reports also the peak values in three cross sections. In a deterministic context (current code, e.g. Eurocode 8) results of this type would be averaged

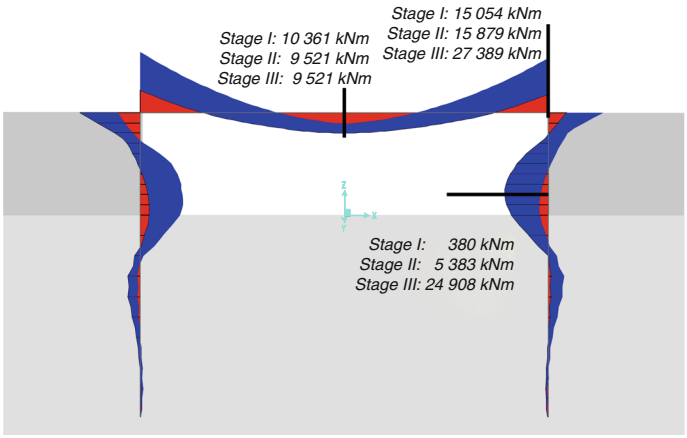

Fig. 5 Bending moment dynamic envelope for record #17

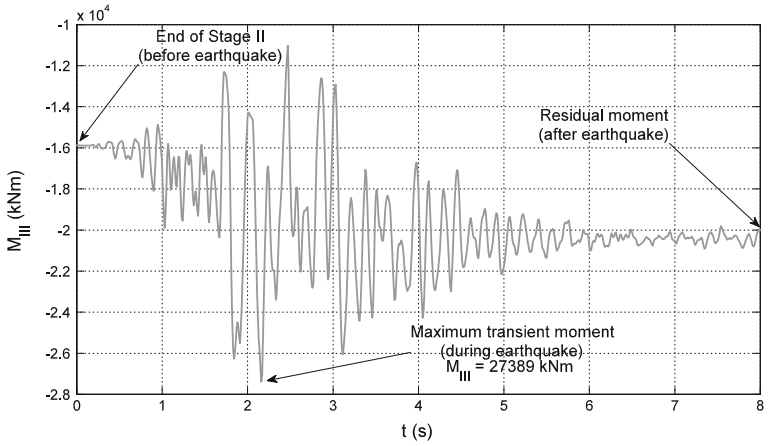

Fig. 6 Bending moment at the abutment-deck connection: time-series for the "mean model" under input signal n.17 highlighting the ratcheting effect and moment build-up

with those of other 6 records (the suite being selected to be compatible with a code spectrum with assigned mean return period) to yield the design action effect. In the context of the illustrated probabilistic procedure, the above result becomes one of 20 points in the intensity *vs* moment increment ΔM plane, as far the seismic moment increment is concerned, and one of the 20 values used to evaluate the parameters of the distribution of M_{II}.

Figure 6 shows the time-series of the bending moment at the right deck-abutment connection during record #17 (the same as in Fig. 5). One can see the non-symmetric response with accumulation of negative moment caused by the cyclic compaction of the soil behind the abutment. The final permanent moment of about 20,000 kNm is considerably larger than the initial one (end of Stage II, $M_{II} = 15,879$ kNm)

As far as the choice of the IM is concerned, spectral acceleration at the fundamental period of the system (in this case equal to $T_1 = 0.486$ s, very close to the value obtained from the simple expression for a homogenous soil deposit $T_1 = 4z_b/V_S = 0.443$ s using the average value over 50 m: $V_S = 361$ m/s) is generally considered to be a *sufficient* and *efficient* intensity

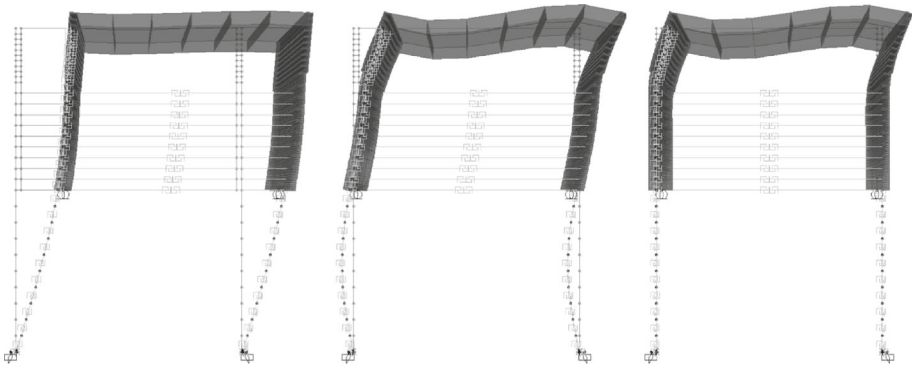

Fig. 7 First three mode shapes and associated vibration periods for the soil–embankment–structure system

measure for peak responses of stable hysteretic systems, meaning that system response is approximately conditionally independent of magnitude and distance, and that the data points show a reduced scatter, when records are scaled to this measure (Padgett et al. 2008).

As already shown in Fig. 6, the analyzed system exhibits a moderate tendency to progressive build-up of stresses and deformations due to the already mentioned "ratcheting" effect. For systems prone to cumulative damage, such as degrading and geotechnical systems, better intensity measures should account for duration (number of significant cycles) and the energy content of the record. Arias intensity, for example, is one such a measure.

Further, one can also note from Fig. 6 that the predominant period of the structural response is about 0.16 s. The latter does not coincide with the fundamental period of the soil deposit but, rather, it is intermediate between the second ($T_2 = 0.19$ s) and third ($T_3 = 0.15$ s) mode periods. This indicates that these modes are better correlated with structural response and thus, spectral acceleration at $T = 0.16$ s may be a much more efficient IM than $S_a(T_1)$. This hypothesis is also supported by the inspection of the first three mode shapes, shown in Fig. 7, which reveals that the latter two modes are those imposing largest flexural deformation on the structure. In particular, the figure allows appreciating how both modes are strictly related to the embankment amplification of motion.

In sum, three candidate IMs are selected as conditioning variable for Eqs. (18, 19). Table 2 reports the values of the three intensity measures for each of the twenty records, the corresponding responses for both the mean and the random model, and the sampled soil and embankment properties for the random model. The latter values have been sampled using the Nataf distribution (Pinto et al. 2004). The correlation coefficient ρ' between the underlying standard normal variables is taken equal to that between the original variables ρ (Liu and Kiureghian 1986).

Figures 8, 9 and 10 show the scatter plots of the IM-ΔM data points for the three selected intensity measures. The figures report the median (solid) and the 16 and 84 % fractile (dashed) curves obtained by power-law fit of the data (Eq. 21), for both the mean and the random model. Table 3 reports the corresponding regression parameters a, b and β.

Starting with Fig. 8 and the data in the table, one can see that, as anticipated, $S_a(T_1)$ is not an efficient IM, since the dispersion for the *mean* model (i.e. the dispersion induced solely by the record-to-record variability) and the *random* model equal 0.58 and 0.50, respectively.

Table 2 Samples of soil and embankment properties, intensity measures and response bending moment at the right deck-abutment connection for the twenty runs

Run	Soil properties (random model)				Seismic input			Mean model			Random model		
	Foundation		Embankment		Intensity			Bending moments (kNm)			Bending moments (kNm)		
	c	$\phi(^\circ)$	V_s(m/s)	$\phi(^\circ)$	$S_a(T_1)$(g)	I_A(m/s)	$S_a(0.16S)$(g)	M_{II}	M_{III}	ΔM	M_{II}	M_{III}	ΔM
1	211	32.4	238	28.9	0.42	0.052	0.31	15,879	20,328	4,449	15,608	20,206	4,598
2	174	32.2	213	30.9	0.09	0.053	0.53	15,879	21,648	5,769	15,828	21,584	5,756
3	133	29.5	295	31.7	0.14	0.012	0.15	15,879	17,925	2,046	16,242	18,418	2,176
4	198	31.2	210	28.3	0.14	0.036	0.39	15,879	20,113	4,234	15,675	18,911	3,236
5	174	28.8	243	30.5	0.20	0.082	0.16	15,879	17,932	2,053	15,872	18,495	2,623
6	124	28.2	209	28.0	0.19	0.066	0.09	15,879	17,504	1,625	16,335	18,577	2,242
7	194	32.9	207	28.7	0.17	0.171	0.17	15,879	18,908	3,029	15,675	19,172	3,497
8	138	29.0	265	30.9	0.63	0.218	0.23	15,879	19,920	4,041	17,224	25,513	8,289
9	161	27.7	245	30.0	0.08	0.007	0.04	15,879	16,687	808	15,976	16,878	902
10	146	27.5	232	30.2	0.16	0.029	0.24	15,879	19,344	3,465	16,112	19,411	3,299
11	198	30.3	209	28.8	0.43	0.065	0.32	15,879	20,595	4,716	15,691	20,034	4,343
12	169	29.4	220	28.8	0.36	0.184	0.29	15,879	20,819	4,940	15,875	22,131	6,256
13	178	29.7	271	31.4	0.12	0.095	0.57	15,879	23,167	7,288	15,849	22,146	6,297
14	186	31.8	213	29.8	0.16	0.054	0.23	15,879	20,671	4,792	17,221	21,682	4,461
15	215	32.4	275	30.7	0.65	0.451	0.52	15,879	25,118	9,239	17,221	27,578	10,357
16	112	27.1	242	29.5	0.14	0.021	0.13	15,879	17,989	2,110	16,548	19,798	3,250
17	180	29.0	238	29.6	0.45	0.405	1.13	15,879	27,389	11,510	17,006	28,936	11,930
18	201	31.8	252	30.8	0.09	0.010	0.10	15,879	17,621	1,742	15,681	17,685	2,004
19	212	29.9	294	31.7	0.24	0.077	0.27	15,879	21,043	5,164	16,923	21,794	4,871
20	156	28.1	242	30.3	0.09	0.103	0.67	15,879	22,651	6,772	16,013	23,822	7,809

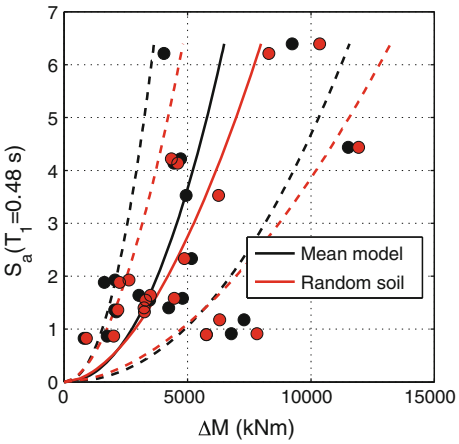

Fig. 8 Scatter plot and power law fit of the intensity-demand (seismic moment increment) relation, obtained for the spectral acceleration at the fundamental system period

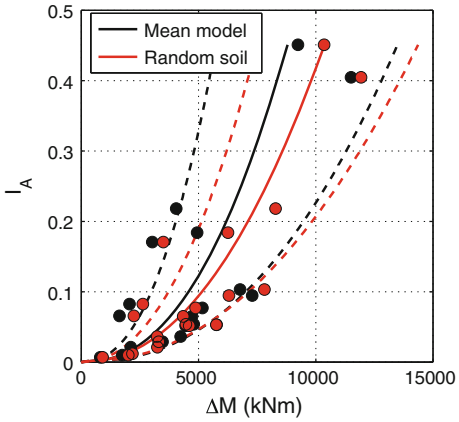

Fig. 9 Scatter plot and power law fit of the intensity-demand (seismic moment increment) relation, obtained for the Arias intensity

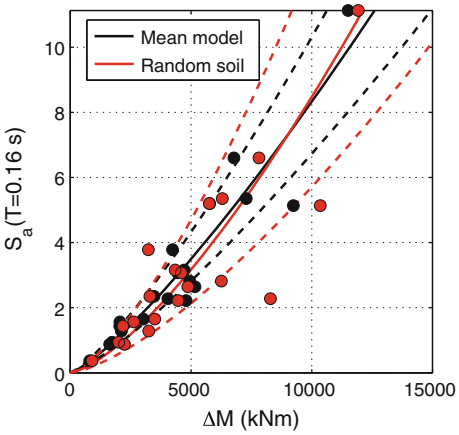

Fig. 10 Scatter plot and power law fit of the intensity-demand (seismic moment increment) relation, obtained for the spectral acceleration at period T = 0.16 s

Interestingly, one would expect the values to be in reverse order, but this counterintuitive result is not meaningful since the difference between these two large values is not statistically significant. The main effect of the increased uncertainty (model uncertainty), with this IM, is

Table 3 Regression parameters of seismic moment increment vs seismic intensity

	$S_a(T_1 = 0.48\,s)$		Arias intensity I_A (m/s)		$S_a(T = 0.16\,s)$	
	Mean model	Random soil	Mean model	Random soil	Mean model	Random soil
a	2,739	2,861	12,422	15,016	1,843	2,218
b	0.46	0.55	0.43	0.46	0.80	0.70
β	0.58	0.50	0.43	0.36	0.17	0.28

to induce an increase in the median ΔM vs IM. The same holds also for the results in Fig. 9. The latter, and the values in Table 3, show that, as expected, the Arias intensity is more efficient than the spectral acceleration at the fundamental period of the system. The dispersion for both models are lower than the previous ones: 0.43 and 0.36, respectively. These values, however, are still rather large and since ground motion prediction equations for I_A, needed to evaluate the corresponding hazard in Eqs. (18) or (19), are generally characterized by a larger dispersion with respect to those for S_a, this IM does not represent a better alternative.

Figure 10 and the results in Table 3 confirm that using the spectral acceleration at a period closer to those of the higher modes dominating the structural response is a far better choice. The $S_a(T = 0.16\,s)$ is highly efficient, especially for the *mean* model, with a dispersion of only 0.17. This spectral IM is even more efficient than the duration-related Arias intensity. This is due to the fact that even if the pressures behind the abutments exhibit a tendency to cumulative build-up, the IAB is still globally symmetric, as opposed e.g. to a free-standing diaphragm-wall (Franchin and Cavalieri 2013), thus limiting the extent to which internal forces can drift.

For this IM, differently from the previous cases, inclusion of model uncertainty leaves the median unchanged and inflates the dispersion that almost doubles to 0.28. The latter value corresponds approximately to the value that could be estimated assuming a linear relationship between the response and the input random variables, consistently with the fact that b for this IM is closer to 1 (0.8 and 0.7, for the mean and random model, respectively), as shown by:

$$\begin{aligned}\sigma_{\ln \Delta M,\text{random}} &= \sqrt{\sigma^2_{\ln \Delta M,\,\text{mean}} + \delta^2_{V_{Se}} + \delta^2_{\phi_e} + \delta^2_{\phi_s} + \delta^2_c} \\ &= \sqrt{0.17^2 + 0.11^2 + 0.04^2 + 0.06^2 + 0.19^2} = 0.286 \end{aligned} \tag{25}$$

where the fact that the standard deviation of the logarithm and the coefficient of variation are numerically equivalent for values lower than 0.3 has been used, and the coefficient of variation of the generic input random variable (uniform in [a,b]) is given by $\delta = \sigma/\mu = (b - a)/\sqrt{12})/((a + b)/2)$.

The data in Table 3 and the power-law for ΔM (*random* model) on $S_a(T = 0.16\,s)$ allow the determination of $\mu_{\ln M_{II}} = 9.69$ kNm, $\sigma_{\ln M_{II}} = 0.035$ and $\rho_{\ln \Delta M|S_a=y,\ln M_{II}} = 0.63$. Figure 11 shows the final result of the procedure for the evaluation of the response MAF curve. The plot shows three MAF curves. The curves labeled "Mean model" and "Random soil" are obtained using Eqs. (19) and (18), respectively, with the seismic hazard curve for the site of the bridge in terms of $S_a(T = 0.16\,s)$, and the demand-intensity parameters in Table 3. The hazard curve has been obtained from data in terms of uniform hazard spectra at 9 return periods (30–2,475 years) supplied for the whole Italian territory by the National Institute of Geophysics and Volcanology. The two curves are close to each other, as expected due to the observed $_{minor}$ effect of system-related uncertainty. This is numerically confirmed by the

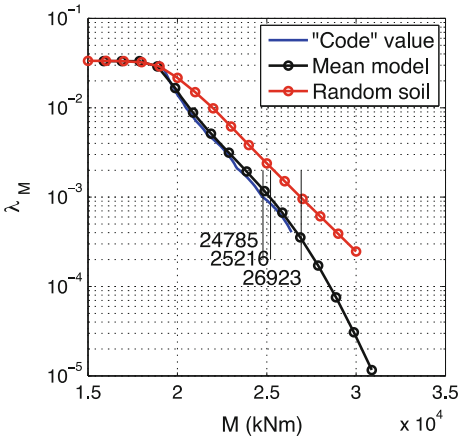

Fig. 11 Mean annual frequency of exceedance: spectral acceleration ("seismic hazard", *left*), total (gravity + seismic) moment (*right*)

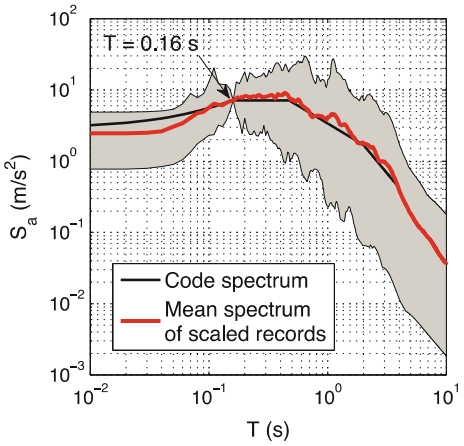

Fig. 12 Response spectra of the 20 selected motions: the *grey band* shows the interval of variation of the individual records spectra

reduced increase in the design value for the connection bending moment. Assuming for the design moment a target MAF of 1/1,000 years, the frequency characterizing the seismic action in the current Italian code for ultimate limit state design under seismic action of ordinary highway structures, the increase from 25,216 (mean model) to 26,923 kNm (random model) is just 7 %.

To put the above results in perspective, the above design values are also compared with a close estimate of the value one would obtain by the current design code in Italy (which is aligned with the Eurocodes). According to the code, when using time-history analysis for response determination, the design action effects equal the mean of the maxima obtained from (at least) seven motions selected to be spectrum compatible (on average) with the 1,000-years uniform hazard spectrum for the site. Further, all analyses shall be carried out on the same model with mean material properties. Thus, the "code value" of the design moment has been estimated from the MAF curve of M_{III} evaluated neglecting all uncertainty other than that in the seismic intensity S_a, described by the hazard curve, i.e. setting $\beta = 0$ and using "Mean model" parameters. This is equivalent to disregarding the system uncertainty (mean model parameters) and taking the mean (actually, the median) of the intensity-demand relationship. The corresponding value on this curve for the accepted frequency of 10^{-3} (equal

to 24,785 kNm) can be taken as a close approximation of the code value, since, as shown in Fig. 12, the selected records, scaled to the 1,000-years value of $S_a(0.16\ s)$ closely match the uniform hazard spectrum from the code with the same return period. The value is practically coincident (just 2 % lower) with that obtained with the probabilistic approach with the mean model, indicating once again the efficiency of the chosen IM.

Finally, the full probabilistic design would be completed by consideration of the uncertainty in the moment capacity. This could be done, as already mentioned, by designing the mean moment capacity (i.e. the flexural strength evaluated with mean material properties) for the demand moment $M_{III} = 26{,}923$ kNm, amplified by a factor $\exp(0.5\ \beta_C^2 k/b)$, whose value in this application is close to one but that can be up to about 1.15 (Cornell et al. 2002).

5 Conclusions

Integral abutment bridges have been built in some areas for decades now, and they are recently experiencing increasing worldwide diffusion in the short to mid-range lengths. Their analysis and design is quite challenging, since it requires consideration of the interaction between foundation soil, structure and backfill even for the deck design under service loads. Cyclic deformations, thermal and most importantly seismic, typically lead to an increase in stresses in the abutments and connections, due to progressive compaction (ratcheting) of the backfill soil, a problem magnified when the bridge is comprised between embankments, whose response amplifies the input motion and drives the deformation of the bridge.

This paper presents a method of analysis and design that is feasible in practice, but still captures the essential physical aspects of the response. Moreover the method is fully performance-based in that displacements and stress resultants (transient and cumulative) can be evaluated accounting for the uncertainties affecting the problem: in the action as well as in the system (foundation, embankments, structure).

The method is based on a simplified inelastic dynamic model for the response determination via inelastic response history analysis, and on approaches to probabilistic seismic assessment of structures that are by now well-established.

The model, developed for implementation in typical commercial analysis packages, employs 1D inelastic site-response analysis and inelastic Winkler-like springs, to capture the main physical aspects of the seismic response of IABs. In particular, the model is based on a global approach to SSI, with the foundation soil profile and overlying embankment modelled explicitly as part of the system. This global approach is the most efficient to reproduce the time-varying imposed displacement along the abutment wall and piles.

A few tens of analyses with carefully selected real recorded motions and associated realizations of system parameters provide a sample of the response that is used for probabilistic demand characterization.

One example application to a highway overpass in Italy illustrates the method. The application, even in its simplicity, has highlighted some interesting findings. The response of the IAB comprised between embankments is indeed driven by their deformation, as already shown in previous studies. In particular, the mode shapes corresponding to the amplification of the free-field motion by the embankments are those inducing maximum flexural deformations in the bridge structure. This has an important practical consequence for the probabilistic assessment. The spectral acceleration at a period close to the periods of these higher modes of vibration (in the example the second and third) turns out to be a very efficient intensity measure, leading to quite reduced dispersion in the intensity-demand relation. This spectral IM has been found to be even more efficient than the duration-related Arias intensity. This is

due to the fact that even if the structural response exhibits a tendency to cumulative build-up of internal forces, the IAB is still globally symmetric, as opposed e.g. to a free-standing diaphragm-wall.

Finally, the application has also shown how consideration of model uncertainty increases the MAF of exceedance of the response and thus the design values of the action effects. This increase is limited in the particular application ($< 10\,\%$), owing to the simplicity of the considered soil profile (homogenous, rather than layered) and of the uncertainty model adopted for illustration (which produces always smooth profiles of the soil properties), as well as to the relatively low variability of the input random variables.

References

Akiyama H, Kajikawa Y (2008) Fundamentally structural characteristics of integral bridges. Thesis, Graduate School of Natural Science & Technology Kanazawa University (http://dspace.lib.kanazawa-u.ac.jp/dspace/bitstream/2297/9646/1/TE-THESIS-AKIYAMA-H-173.pdf)

ATV-6 (1996a) Seismic design guidelines for highway bridges. Applied Technology Council, Redwood City

ATC-32 (1996b) Improved seismic design criteria for california bridges: provisional recommendations. Applied Technology Council, Redwood City

Baker JW, Cornell CA (2006) Spectral shape, epsilon and record selection. Earthq Eng Struct Dyn 35:1077–1095

Baptiste KT, Kim W, Laman JA (2011) Parametric study and length limitations for prestressed concrete girder integral abutment bridges. Struct Eng Int 21(2):151–156

Becci B, Nova R (1987) A method for analysis and design of flexible sheetpiles. Rivista Italiana di Geotecnica 1(87):33–47 (in Italian)

Benjamin JR, Cornell CA (1970) Probability, statistics, and decision for civil engineers. McGraw-Hill, New York

Bouc R (1971) Modèle matematique d'hysteresis. Acustica 21:16–25

Burke MP (2004) Integral bridge design is on the rise. AISC Mod Steel Constr 30(4):9–11

Caltrans SDC (1999) Caltrans seismic design criteria version 1.1. California Department of Transportation, Sacramento

CEN European Committee for Standardization (2004) EN1998-1 design of structures for earthquake resistance part 1 general rules, seismic actions and rules for buildings. Brussels, Belgium

CEN European Committee for Standardization (2005) EN1998-2 design of structures for earthquake resistance part 2 bridges. Brussels, Belgium

Connal J (2004) Integral abutment bridges-Australian and US practise. 5th Austroads bridge conference, Hobart, Tasmania

Cornell CA (1996) Reliability-based earthquake-resistant design; the future. 11th world conference on earthquake engineering (paper 2166), Acapulco, Mexico

Cornell CA, Krawinkler H (2000) Progress and challenges in seismic performance assessment. PEER News 3(2):1–3

Cornell CA, Jalayer F, Hamburger RO, Foutch DA (2002) The probabilistic basis for the 2000 SAC/FEMA steel moment frame guidelines. ASCE J Struct Eng 128(4):526–533

CSI Computer & Structures Inc (2009) Sap 2000 analysis reference manual. Berkely

Dicleli M (2005) Integral abutment-backfill behavior on sand soil—pushover analysis approach. J Bridge Eng 10:354–364

Dicleli M, Erhan S (2011) Effect of foundation soil stiffness on the seismic performance of integral bridges. Struct Eng Int 21(2):162–168

Drosos VA, Gerolymos N, Gazetas G (2012) Constitutive model for soil amplification of ground shaking: parameter calibration, comparisons, validation. Soil Dyn Earthq Eng 42:255–274

Elgamal AW, Yang Z, Parra E, Ragheb A (1998) Cyclic 1D: an internet-based finite-element computer program for one-dimensional site amplification analysis using an incremental plasticity coupled solid-fluid formulation. University of California, San Diego

Elgamal AW, Yan L, Yang Z, Conte JP (2008) Three-dimensional seismic response of Humboldt Bay bridge-foundation-ground system. ASCE J Struct Eng 134(7):1165–1176

England GL, Tsang NCM, Bush DI (2000) Integral bridges: a fundamental approach to the time-temperature loading problem. Thomas Telford, London

Franchin P, Pinto PE, Noto F (2007) A simplified nonlinear dynamic model for seismic analysis of earth-retaining diaphragm-walls. 4th ICEGE (paper 1220), Thessaloniki, Greece
Franchin P, Cavalieri F (2013) Performance-based seismic design of flexible earth-retaining structures, 11th ICOSSAR. New York
Gerolymos N, Gazetas G (2005) Constitutive model for 1-D cyclic soil behaviour applied to seismic analysis of layered deposits. Soils Found 45(3):147–159
IIC International Code Council (2012) International building code. ISBN: 9781609830403
Ishibashi I, Zhang X (1993) Unified dynamic shear moduli and damping ratios of sand and clay. Soils Found 33(1):182–191
Kaufmann W (2011) Swiss federal roads office guidelines for integral bridges. Struct Eng Int 21(2):189–194
Kotsoglou A, Pantazopoulou S (2007) Bridge-embankment interaction under transverse ground excitation. Earthq Eng Struct Dyn 36:1719–1740
Kotsoglou A, Pantazopoulou S (2009) Assessment and modeling of embankment participation in the seismic response of integral abutment bridges. Bull Earthq Eng 7:343–361
Kotsoglou A, Pantazopoulou S (2010) Response simulation and seismic assessment of highway overcrossings. Earthq Eng Struct Dyn 39:991–1013
Kramer SL (1996) Geotechnical earthquake engineering. Prentice-Hall, Englewood Cliffs
Krawinkler H, Miranda E (2004) Performance-based earthquake engineering. In: Bozorgnia Y, Bertero VV (eds) Chapter 9 of "Earthquake engineering: from engineering seismology to performance-based engineering". CRC Press, Boca Raton
Liu P, Der Kiureghian A (1986) Multivariate distribution models with prescribed marginals and covariances. Probab Eng Mech 1(2):105–112
Maruri R, Petro S (2005) Integral abutments and jointless bridges (IAJB) 2004 survey summary, FHWA conference
McKenna F, Fenves GL, Scott MH (2000) Open system for earthquake engineering simulation. University of California, Berkeley
Nakamura S, Momijama Y, Hosaka T, Homma K (2002) New technologies of steel/concrete composite bridges. J Constr Steel Res 58:99–130
Padgett JE, Nielson BG, DesRoches R (2008) Selection of optimal intensity measures in probabilistic seismic demand models of highway bridge portfolios. Earthq Eng Struct Dyn 37:711–725
Pekcan G, Itani A, Monzon E (2010) Seismic design recommendations for steel girder bridges with integral abutments. 89th transportation research board annual meeting, Washington, DC
Pinto PE, Giannini R, Franchin P (2004) Seismic reliability analysis of structures. IUSSPress, Pavia. ISBN 88-7358-017-3
Schnabel PB, Lysmer J, Seed HB (1972) SHAKE: a computer program for earthquake response analysis of horizontally layered sites. Report EERC 72–12, Earthquake Engineering Research Center, University of California, Berkeley
Shome N, Cornell CA, Bazzurro P, Carballo J (1998) Earthquake, records, and nonlinear MDOF responses. Earthq Spectra 14(3):469–500
Spyrakos C, Loannidis G (2003) Seismic behaviour of post-tensioned integral bridge including soil–structure interaction. Soil Dyn Earthq Eng 23:53–63
Vashegani-Farahani R, Zhao Q, Burdette EG (2010) Seismic analysis of integral abutment bridge in Tennessee, including soil–structure interaction. J Transp Res Board 2201:70–79
Wasserman EP (2007) Integral abutment design (practice in the United States. First US-Italy seismic bridge workshop, Pavia, Italy
Wen YK (1976) Method for random vibration of hysteretic systems. ASCE J Eng Mech Div 102(2):249–263
White H II (2007) Integral abutment bridges: comparison of current practice between European countries and The United States of America, special report 152. Transportation Research and Development Bureau, New York State Department of Transportation
White II H, Pétursson H, Collin P (2010) Integral abutment bridges: the European Way. ASCE Pract Period Struct Des Constr 15:201–208
Wilson JC, Tan BS (1990a) Bridge abutments: formulation of a simple model for earthquake response analysis. J Eng Mech 116(8):1828–1837
Wilson JC, Tan BS (1990b) Bridge abutments: assessing their influence on earthquake response of meloland road overpass. J Eng Mech 116(8):1838–1856
Zhang J, Makris N (2002a) Kinematic response functions and dynamic stiffnesses of bridge embankments. Earthq Eng Struct Dyn 31:1933–1966
Zhang J, Makris N (2002b) Seismic response analysis of highway overcrossings including soil–structure interaction. Earthq Eng Struct Dyn 31:1967–1991